Chapter 4

Multi-layer TiO_2 nanotubes-based VOC sensors for high sensitivity and selectivity

4. 1 Introduction

Sensors employing TiO_2 nanotubes usually exhibited less sensitivity and selectivity at room temperature and generally, operated at high temperature (above 100 °C) to detect VOCs [1-8]. Thus, after the identification of VOCs by using both resistive and capacitive sensing, structural and morphological parameters of TiO_2 nanotubes were altered with an aim to get improved sensitivity and selectivity at room temperature. To achieve this goal, multi-layered TiO_2 nanotubes array was synthesized by electrochemical anodization technique where pre-defined voltage pulse(s) were used to append the nanotubes layer(s). Single (one bunch), double (two bunches) and triple (three bunches) layered TiO_2 nanotubes array were synthesized and configured in vertical structured device (Au/TiO_2 nanotube layer(s)/Ti) for detecting a very low concentration (40-160 ppm) of organic vapors. The morphological and structural details of different nanotubes were studied using FESEM and XRD. The growth mechanism for multi-layered TiO_2 nanotubes was also discussed in detail. The resistive and capacitive sensing performance of all three sensors having single, double and triple layers of nanotubes, respectively, were compared in terms of sensitivity, response /recovery time, selectivity and stability.

4. 2 Synthesis of multi-layered TiO_2 nanotubes

Multi-layered TiO_2 nanotubes were synthesized by using step voltage assisted electrochemical anodization technique. The anodization set-up was similar to the set-up discussed in sec. 2.2 (Chapter 2). However, instead of using a constant voltage supply, a pulse assisted voltage supply was used for synthesizing multi-layers of

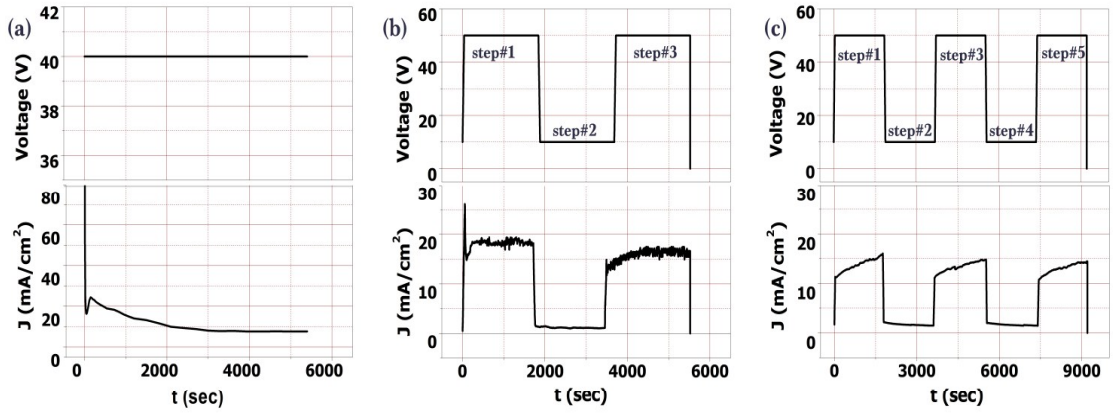

Fig. 4.1 Anodization voltage and current density (J) profile for (a) single layer TiO_2 nanotubes, (b) double layer TiO_2 nanotubes, and (c) triple layer TiO_2 nanotubes.

nanotubes. Ti foil (99.99% pure, 0.25 mm thick) was used as the anode material with affective dimensions of 1.5 cm × 1.5 cm. It was then cleaned with methanol and kept in air ambient to dry. The electrolyte was prepared with 0.5 wt. % of NH_4F, 10 vol. % of DI water and ethylene glycol. All anodization processes were carried out at room temperature (27 °C). Applied anodization voltage and corresponding current density (J) through electrolyte were recorded while synthesizing single, double and triple layered TiO_2 nanotubes and represented in Fig. 4.1. Single layered TiO_2 nanotubes were synthesized by applying 40 V constant potential for 90 min (Fig. 4.1 (a)). Multi-layered TiO_2 nanotubes were synthesized by modulating anodization voltage with time where other synthesis parameters were kept constant. In step#1, the anodization voltage was raised up from 10 V to 50 V (rate: +1 V/s) and kept constant for 30 min at 50 V. In step#2, anodization voltage was reduced from 50 V to 10 V (rate: -1V/s) and kept constant for 30 min at 10 V. Step#3 and step#5 were the repetition of step#1; and step#4 was the repetition of step#2 as shown in Fig. 4.1 (b) and (c). Double layered TiO_2 nanotubes were synthesized by using the voltage profile of step#1 → step#2 → step#3 and total anodization time was ~90 min (Fig. 4.1 (b)). Triple layered TiO_2 nanotubes was synthesized by using the voltage profile of step#1 → step#2 → step#3 → step#4 → step#5 and total anodization time was ~150 min (Fig.

4.1 (c)). After anodization, as grown samples were rinsed with DI water and dried in air at room temperature. Samples were then annealed at 330 °C for 3 h in air ambient for increasing the mechanical strength and crystallinity of nanotubes. The morphological and structural details of the annealed samples were characterized by FESEM and XRD, respectively.

4. 3 Experimental setup for VOC sensing

The sensing properties of three different types of sensors (SL-NTs, DL-NTs, and TL-NTs) having single, double and triple layers of TiO_2 nanotubes, respectively were tested in both resistive and capacitive modes. The sensor fabrication steps were similar to the steps discussed in sec. 2.2 (Chapter 2). The sensing properties of all developed sensors were measured at room temperature (27 °C) and 40% relative humidity (RH) in a sealed glass test chamber having electrical feed through. A pico-ammeter (Keithley 6487) was used to measure the conductometric sensing performance at 1 V constant bias voltage. For measuring capacitive sensing, sensors were connected to an LCR meter (as discussed in sec. 2.3). After getting the maximum and saturated response, the sensor was pulled out from the sensing chamber and placed in air ambient for the recovery of sensor. Response (t_{res}) and recovery (t_{rec}) time denote the time taken by the sensor to reach 90% of its steady-state resistive/capacitive response value after injecting and removing of VOC analytes, respectively.

4. 4 Characterizations of single and multi-layered TiO_2 nanotubes

FESEM images of side and top view of single (Fig. 4.2 (a, b)), double (Fig. 4.2 (c, d, e)) and triple (Fig. 4.2 (f, g, h, i)) layered TiO_2 nanotubes are shown in Fig. 4.2. A wide view of the samples depicts porous, highly oriented one-dimension and vertically aligned nanotubes. Table 4.1 summarizes the length, inner diameter and wall thickness of TiO_2 nanotubes. The maximum length of individual layer of nanotubes was found

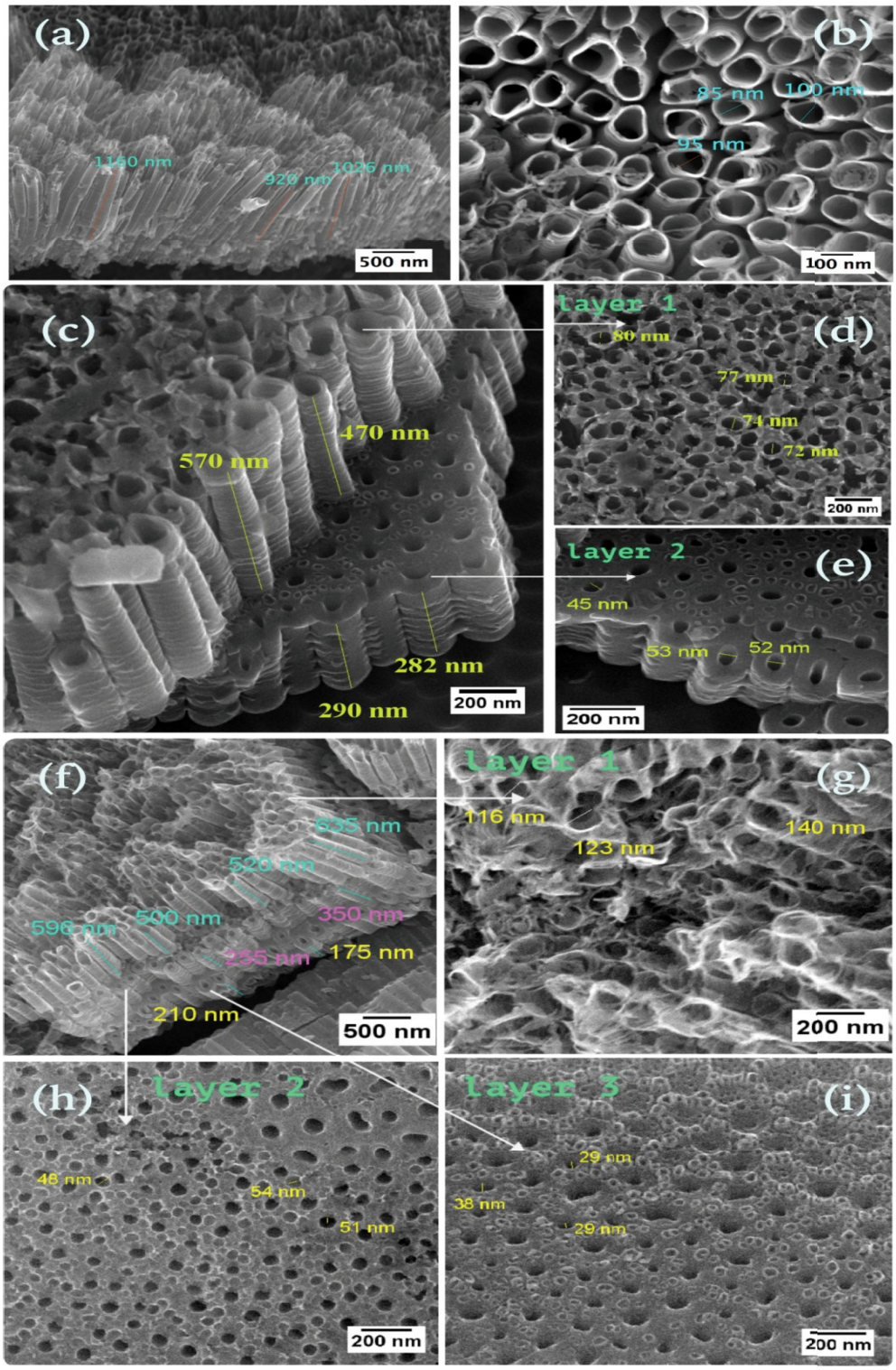

Fig. 4.2 FESEM images of single and multi-layered nanotubes. SL-NTs: (a) side view, and (b) top view. DL-NTs: (c) side view, (d) top view of first layer, and (e) top view of second layer. TL-NTs: (f) side view, (g) top view of first layer, (h) top view of second layer, and (i) top view of third layer.

Table 4.1 Morphological parameters of TiO_2 nanotubes from FESEM study.

Parameters	*Layer(s)*	*Single Layered (SL-NTs)*	*Double Layered (DL-NTs)*	*Triple Layered (TL-NTs)*
Length (nm)	First/Initial	900-1180	470-580	520-650
	Second	------	280-300	250-350
	Third	------	------	175-210
Inner diameter (nm)	First/Initial	85-100	70-80	115-140
	Second	------	45-55	45-55
	Third	------	------	28-38
Wall thickness (nm)	First/Initial	10-12	22-25	8-10
	Second	------	60-85	30-42
	Third	------	------	55-88

to be maximum for SL-NTs. For double and triple layered nanotubes, the length and inner diameter of the nanotubes were maximum for initially grown nanotubes and minimum for finally grown nanotubes. However, the wall thickness was thinnest for initially grown nanotubes and thickest for finally grown nanotubes. These morphological variations in nanotubes can be explained by considering growth kinetics during the anodization process of nanotubes. The oxidation of Ti and oxide dissolution rate were slower in case of the formation of the lowest layer (finally grown) as compared to the upper layer due to restricted diffusion of ion species through upper layered nanotubes. Also, the upper layer of TiO_2 nanotubes was grown first and got relatively more time to get dissolve by F^- ions in form of $[TiF_6]^{2-}$, and thus larger inner diameter and smaller wall thickness (due to etching) were observed. Also, the effectiveness of vertical electric field during anodization was relatively less for the growth of lower layer of nanotubes as already grown top layer hindered the field intensity, and thus responsible for a shorter length of lower layered nanotubes.

XRD patterns of the annealed TiO_2 nanotubes/Ti samples in Fig. 4.3 show two types of peaks, (i) anatase peaks (A) originated from TiO_2 nanotubes layer(s), and (ii)

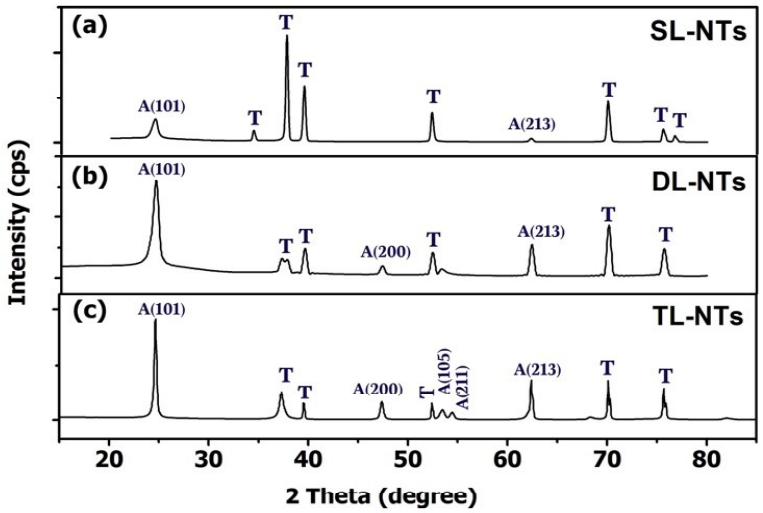

Fig. 4.3 XRD patterns of TiO_2 nanotubes having (a) single layer TiO_2 nanotubes, (b) double layer TiO_2 nanotubes, and (c) triple layer TiO_2 nanotubes.

Ti peaks (T) originated from titanium substrate. As evident from Fig. 4.3, anatase peak intensity was increased and Ti peak intensity was decreased from SL-NTs to TL-NTs. Also, Anatase (101) and Anatase (213) peaks became sharper from single layer to double layer and further in the triple layer. Anatase (200) peak was invisible in SL-NTs but was appeared in the case of multi-layered nanotubes. In the case of SL-NTs, X-rays could penetrate easily through the thin walls of nanotubes and hence gave more substrate information with high intensity titanium peaks. In DL-NTs, wall thickness of the second layer was relatively higher and X-rays could not able to penetrate as much as in SL-NTs resulting in suppressed peaks of the substrate. For TL-NTs, information about the Ti substrate was further attenuated as wall thickness of the lowest layer of TL-NTs was maximum. The crystalline size of anatase (101) phase was measured by using Scherrer's equation [9]. The average crystalline size was increased from 13.2 nm to 20 nm and to 34.5 nm as the number of TiO_2 nanotubes layer was increased from single to double and to triple, respectively. So, the overall XRD result supports the morphological features of different TiO_2 nanotubes envisaged from FESEM images. The growth of multi-layers of nanotubes during anodization relies on various physical and chemical factors which are discussed in detail in the next section.

4. 5 Growth mechanism of multi-layered TiO_2 nanotubes

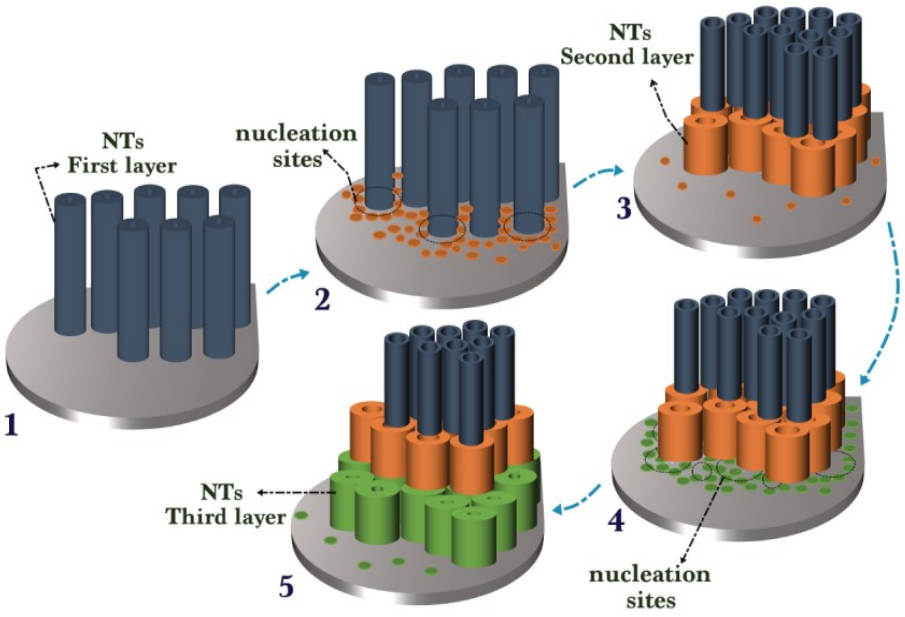

Fig. 4.4 A schematic of the steps involved in the growth of multi-layered TiO_2 nanotubes.

Fig. 4.4 shows a schematic of the stages involved in the growth of double and triple layered nanotubes. Anodic voltage profile of step#1 to step#5 is shown in Fig. 4.1. In step#1, the first layer of TiO_2 nanotubes was grown on the Ti substrate due to constant 50 V. The growth of these nanotubes was the result of field assisted oxidation and dissolution [10]. In step#2, the ion diffusion gradient was reduced by lowering of anodic voltage from 50 V to 10 V, and thus field assisted nanotube synthesis was restricted. At this lower field, pits and pores formation was continued in between the gaps of existing nanotubes. Thus, these pits and pores facilitated the seeding or nucleation sites for the formation of the second layer of nanotubes as shown in step#2. In step#3, due to an increase of anodic voltage from 10 V to 50 V again, the second layer of nanotubes was started to grow from the developed nucleation sites. The processes involved in step#4 and #5 were replicated with step#2 and step#3, respectively and hence three layers of nanotubes were grown. During anodization, the top layer of nanotubes was formed first and had the longest exposure to electrolyte

which was responsible for more dissolution of TiO_2. Therefore, the wall thickness of nanotubes was the thinnest for top layer than second and third layers. Incorporation of electrolyte on Ti substrate became difficult with increase of number of layer(s) that restricted the formation of nucleation sites for next layer. So, the density of nanotubes became very less in the case of bottom layers [11].

4. 6 Comparative sensing study of single and multi-layered TiO_2 nanotubes-based sensors

4. 6. 1 Resistive sensing performance

Table 4.2 Resistance of the sensor upon exposure to 40-160 ppm of ethanol at room temperature.

S. No.	*Type of sensor*	*Base-line resistance (MΩ)*	*Resistance (MΩ)*			
			in 40 ppm ethanol	*in 80 ppm ethanol*	*in 120 ppm ethanol*	*in 160 ppm ethanol*
1	SL-NTs	9.6	7.8	6.3	5.7	4.3
2	DL-NTs	43.4	29.1	16.8	5.32	3.28
3	TL-NTs	57.5	32.8	9.15	4.2	2.7

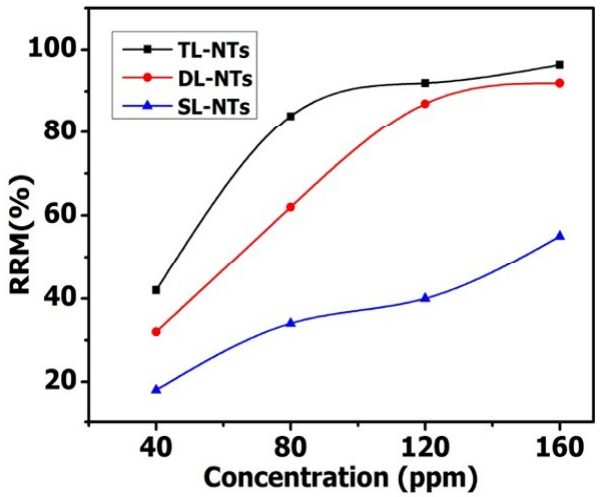

Fig. 4.5 Resistive response magnitude as a function of ethanol concentration for three different sensors tested at room temperature (27 °C).

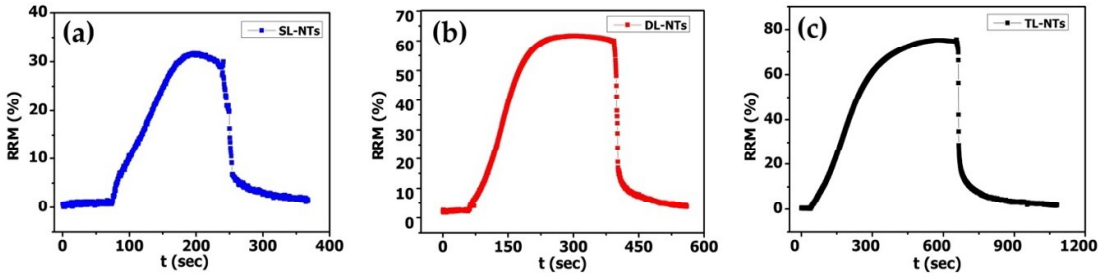

Fig. 4.6 Transient behavior of (a) single, (b) double, and (c) triple layered nanotubes-based sensors in presence of 80 ppm of ethanol at 27 °C.

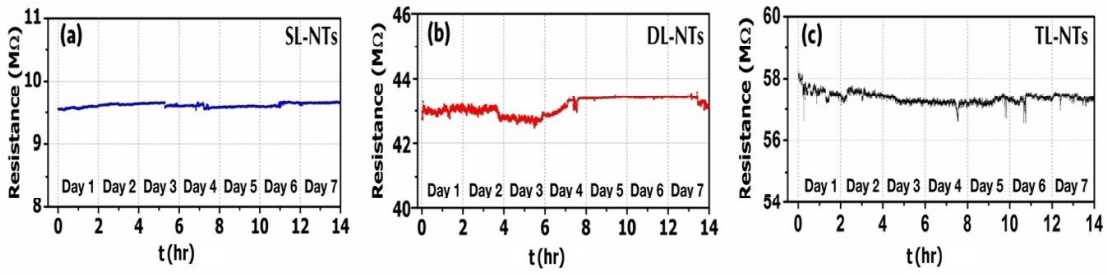

Fig. 4.7 Baseline resistance stability test of (a) single, (b) double, and (c) triple layered nanotubes-based sensors operating at 27 °C in air ambient over a span of seven days.

Table 4.2 lists the baseline resistances and resistance change in the exposure of 40-160 ppm of ethanol at room temperature for SL, DL and TL-NTs. Resistive response magnitude (RRM) of the sensors at room temperature as a function of ethanol concentration for three types of nanotubes is plotted in Fig. 4.5. TL-NTs sensor has shown the highest response of 96% at 160 ppm of ethanol. The response of DL-NTs sensor was also promising where 92% response was recorded at 160 ppm of ethanol. For both double and triple layered nanotubes-based sensor, responses were saturated at higher concentrations (>120 ppm). The lowest and almost linear response was observed for SL-NTs sensor when exposed to ethanol (40 to 160 ppm).

The transient behavior of all three sensors at room temperature upon exposure to 80 ppm of ethanol is shown in Fig. 4.6. Resistive response magnitude (RRM), response time (t_{res}) and recovery time (t_{rec}) were increased from single (RRM= 31%, t_{res}= 82 s, t_{rec}= 39 s) to double (RRM= 62%, t_{res}= 141 s, t_{rec}= 52 s) to triple (RRM= 74%, t_{res}= 290 s, t_{rec}= 80 s) layered nanotubes sensors. The long-term stability of the

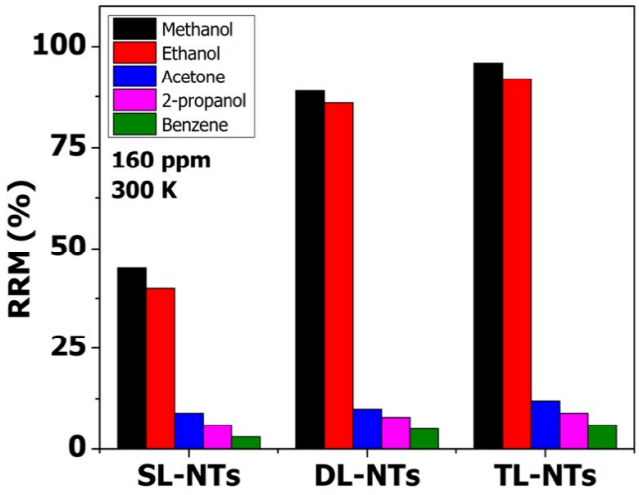

Fig. 4.8 Comparative resistive response magnitude (RRM) of SL, DL, TL-NTs based sensors towards 160 ppm of methanol, ethanol, acetone, 2-propanol, and benzene at 27 °C.

sensors operating at room temperature (27 °C) were tested by measuring baseline resistance in air ambient over a span of seven days as shown in Fig. 4.7 (a)–(c). As evident, SL-NTs sensor has shown the best stability in terms of its baseline resistance compared to DL-NTs and TL-NTs. The maximum deviation in baseline resistance of the sensor was found to be ±0.1 MΩ, ±1 MΩ, and ±1.5 MΩ for SL-NTs, DL-NTs, and TL-NTs, respectively. The resistive sensing performance of all three sensors was tested for other VOCs also like methanol, acetone, 2-propanol, benzene at room temperature and response at 160 ppm of their respective concentration is represented in Fig. 4.8. As evident, methanol has shown the maximum resistive response magnitude for all three types of sensors. However, all three sensors had poor selectivity for methanol with respect to ethanol.

4. 6. 2 Capacitive sensing performance

Similar to the resistive response study, Table 4.3 lists the baseline capacitance and capacitance change in the exposure of 40-160 ppm of ethanol at room temperature for SL, DL, and TL-NTs. Capacitive response magnitude (CRM) of the sensors at room

Table 4.3 Capacitance of the sensor upon exposure to 40-160 ppm of ethanol at room

temperature.

Sl. No.	*Type of sensor*	*Base-line capacitance (pF)*	*Capacitance in 40 ppm (pF)*	*Capacitance in 80 ppm (pF)*	*Capacitance in 120 ppm (pF)*	*Capacitance in 160 ppm (pF)*
1	SL-NTs	14.5	24.65	30.45	37.7	49.3
2	DL-NTs	59.3	88.95	103.775	117.414	140.541
3	TL-NTs	70.9	106.35	124.075	140.382	168.033

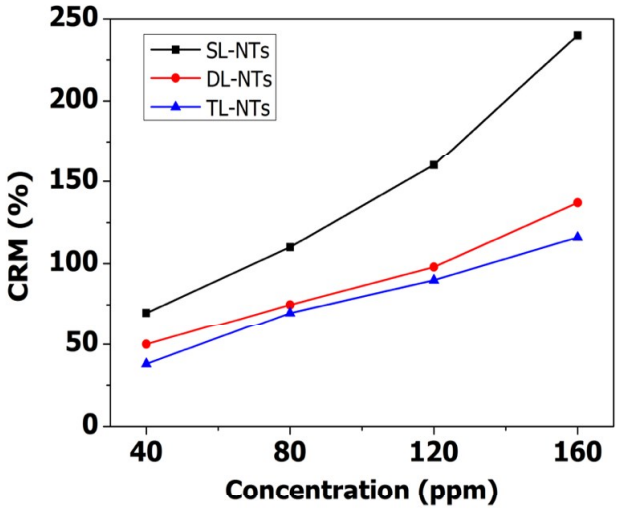

Fig 4.9 Capacitive response magnitude (CRM) as a function of ethanol concentration for three different sensors tested at room temperature (27 °C).

temperature as a function of ethanol concentration for all three types of nanotubes is plotted in Fig. 4.9. SL-NTs sensor had the highest capacitive response of 240% at 160 ppm of ethanol. However, CRM of DL-NTs sensor was decreased to 137% at 160 ppm of ethanol. For TL-NTs, CRM was reduced further to 116% at 160 ppm of ethanol. Thus, it was noticed that CRM was degraded with an increase in the number of layers of nanotubes, unlike RRM.

The transient behavior of the capacitive responses of all three sensors upon exposure to 80 ppm of ethanol at room temperature is shown in Fig. 4.10. Response time (t_{res}) and recovery time (t_{rec}) were increased from single (t_{res}= 253 s, t_{rec}— 12 s) to

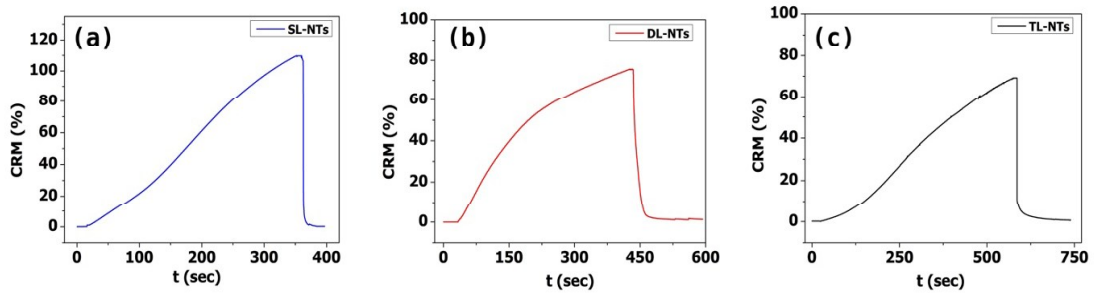

Fig. 4.10 Transient behavior of capacitive response for (a) single, (b) double, and (c) triple layered nanotubes-based sensors in presence of 80 ppm of ethanol at 27 °C.

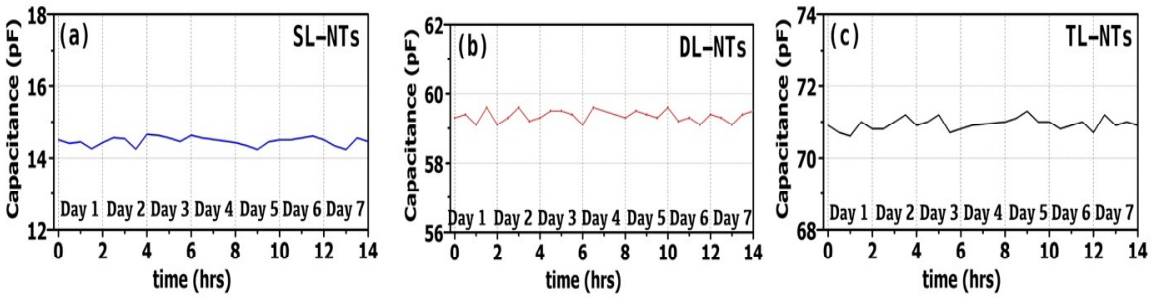

Fig. 4.11 Baseline capacitance stability test of (a) single, (b) double, and (c) triple layered nanotubes- based sensors operating at 27 °C in air ambient over a span of seven days.

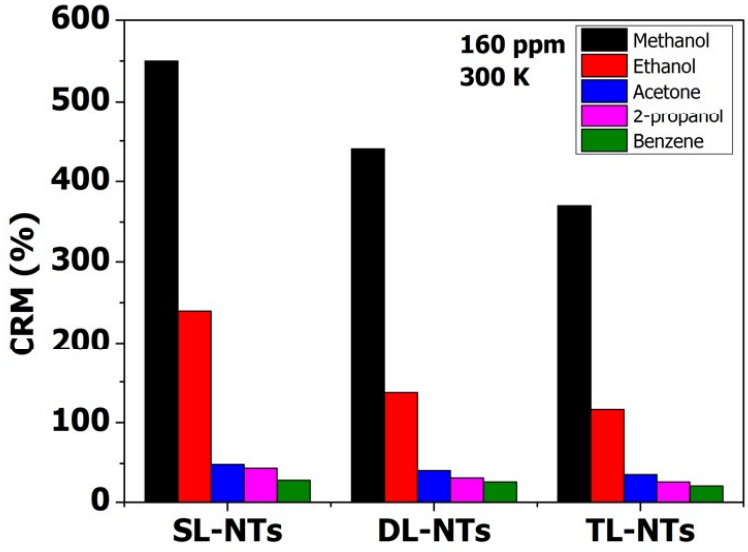

Fig. 4.12 Comparative capacitive response magnitude (CRM) of SL, DL, TL-NTs based sensors towards 160 ppm of methanol, ethanol, acetone, 2-propanol, and benzene at 27 °C.

double (t_{res}= 277 s, t_{rec}= 18 s) to triple (t_{res}= 370 s, t_{rec}= 26 s) layered nanotubes sensors. The long-term stability of the sensors operating at room temperature (27 °C)

was tested by measuring the baseline capacitance in air ambient over a span time of seven days as shown in Fig. 4.11 (a)–(c). As evident, SL-NTs sensor has shown the best stability in terms of its baseline resistance compared to DL-NTs and TL-NTs. The maximum deviation in baseline resistance was found to be ±0.3 pF, ±0.6 pF, and ±0.4 pF for SL-NTs, DL-NTs, and TL-NTs, respectively. The capacitive sensing performance of all three sensors was tested for other VOCs like methanol, acetone, 2-propanol, benzene at room temperature and response at 160 ppm of their respective concentration is represented in Fig. 4.12. As evident, methanol has shown the maximum CRM for all three types of sensors. Also, the sensor exhibited excellent selectivity for methanol with respect to ethanol in the case of capacitive sensing. Relative percentage change in capacitive response for methanol and ethanol was found to be 56.3%, 68.6%, and 68.8% for SL, DL, and TL-NTs based sensors respectively. Hence, improvement in selectivity was observed for multi-layered nanotubes.

4. 7 Sensing mechanism of multi-layered TiO_2 nanotubes-based sensors

The following observations were made from this sensor study i.e. (i.) resistive response magnitude of the sensor was increased and capacitive response magnitude was decreased with the number of layers, (ii.) both baseline resistance and resistance change upon exposure to reducing ambient was increased for a greater number of layers, (iii.) response and recovery time of the sensors became slower with the increase in number of layers, and (iv.) selectivity of the sensor towards methanol improved with number of layers in capacitive mode. All these phenomena are interrelated and can be explained in the following way: In vertical structured device, bias voltage was applied between the top and bottom electrodes (Consider, Au: +ve and Ti: -ve) and the resistance of sensor was originated from three sources i.e. (i.) TiO_2 nanotubes, (ii). junction between two layers of nanotubes, and (iii.) electrode metal/TiO_2 nanotubes junctions. The effect of point (iii.) i.e. metal/TiO_2 nanotubes junction was common for all the three types of sensors, and thus can be neglected from the comparative study.

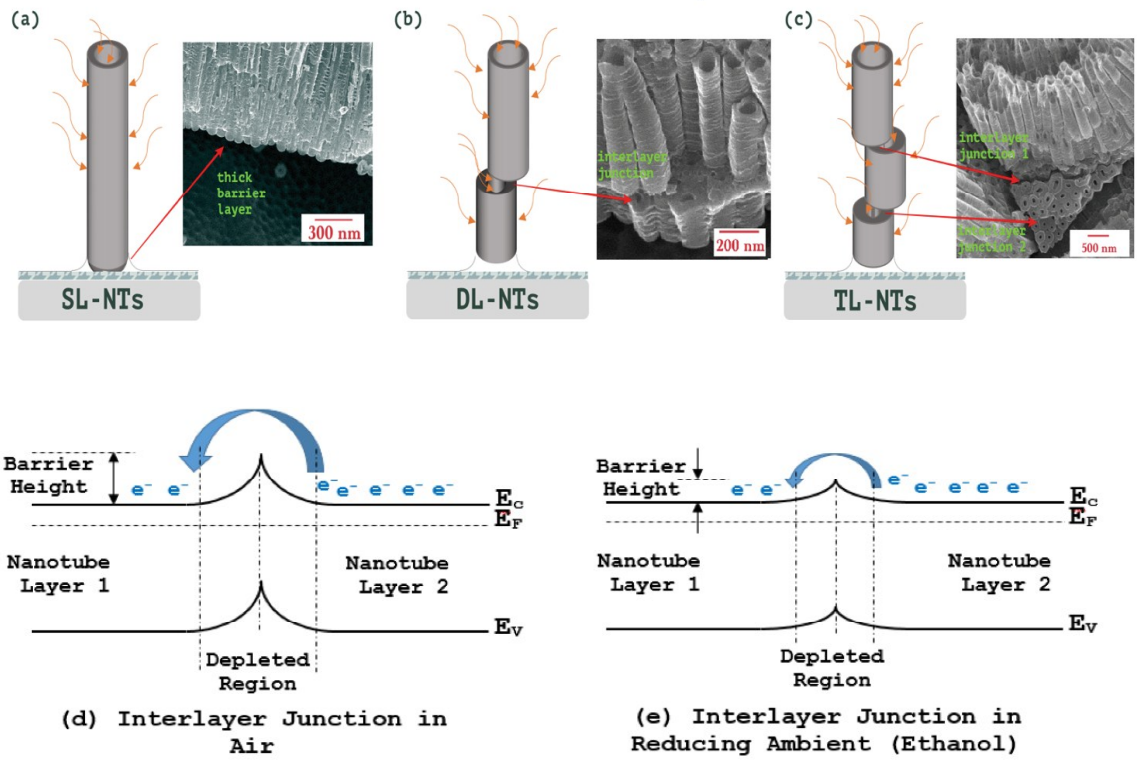

Fig. 4.13 Schematics showing sensing mechanism. (a) SL-NTs, (b) DL-NTs with one interlayer junction, and (c) TL-NTs with two interlayer junctions. Energy band diagrams of Schottky barrier at inter layer junction (d) in air, and (e) in reducing ambient (ethanol).

For SL-NTs, only one layer of TiO_2 nanotubes was responsible for the resistance of sensor (no inter layer junctions) as shown in Fig. 4.13 (a). In DL-NTs, two layers of TiO_2 nanotubes with one inter layer junction(s) were responsible for the resistance of sensor (Fig. 4.13 (b)). In TL-NTs, the resistance of the sensor was originated from three layers of TiO_2 nanotubes with two inter layer junctions as shown in Fig. 4.13 (c). The resistance of individual layers of nanotubes was different because of their non-uniform structure (Table 4.1). The thinner wall of nanotubes offered higher resistance and the thicker wall of nanotubes offered lower resistance. However, if the inter layer junctions were to be focused, a Schottky barrier was observed at the junction of two layers due to the surface depletion by oxygen species in air ambient (Fig. 4.13 (d)) [12]. So, the baseline resistance of double and then triple layered sensor was increased because of the dual effect of additional nanotube layer(s) and developed a potential

barrier at inter layer junctions. The morphology of the multi-layered nanotubes was also responsible for its high resistance and response. In SL-NTs, inner wall of the nanotubes was restricted from external ambient due to surface coverage by top electrode (Au) layer and only the outer walls contributed in sensing. But, in the case of DL-NTs and TL-NTs, access of inner walls of nanotubes was increased extensively because of porous junctions between two layers as clearly shown in Fig. 4.13 (b) and (c). So, the effective surface area gets increased a few times in the case of multi-layered TiO_2 nanotube array that clearly reflected in resistive response behavior of sensors.

Resistive response of the sensor for multi-layered nanotubes was also increased because of Schottky barrier effect at inter layer junction. In reducing ambient, adsorbed oxygen species were removed and extra electrons were added to the surface of nanotubes that significantly lowered the depletion width as well as a potential barrier at inter-layer junction as shown in Fig. 4.13 (e). Therefore, a high resistance change (or high response) was observed in the case of DL and TL-NTs due to (i.) enhanced surface area, and (ii.) Schottky barrier lowering at interlayer junction. An increase in response and recovery time is also obvious for multi-layered nanotubes. With the increase of porosity and effective surface area in multi-layered nanotubes, gas/vapor diffusion time gets increased during the response and recovery process. Therefore, the higher possibility of surface adsorption/desorption results in extended response/recovery time.

In general, capacitance of the sensor depends upon the dielectric medium between two electrodes of the sensor as discussed in sec. 2.5 (Chapter 2). In all three types of fabricated sensors, two different kinds of dielectric mediums were present i.e. free space and TiO_2 nanotubes. For SL-NTs, as evident from FESEM images (Fig. 4.2), free space in between nanotubes were maximum because of thin nanotubes. For DL-NTs, nanotubes get thicker, and thus increment in baseline capacitance of the sensor was observed because of the higher dielectric constant of TiO_2 with respect to free space (Table 4.3). The baseline capacitance further increased for TL-NTs as more space

between two electrodes gets filled with nanotubes. Thus, increasing baseline capacitance with an increase in the number of layers of nanotubes resulted in degradation of the capacitive sensitivity/CRM of the sensor.

For SL-NTs, the sensor showed a higher capacitive response for methanol as compared to ethanol because of the difference in dielectric constant values of these two VOCs. However, in the case of multi-layer nanotubes, although capacitive sensitivity gets reduced with respect to SL-NTs but selectivity towards methanol was found to get increased with increase in number of layers of nanotubes. It is attributed for same ppm level of ethanol and methanol, a greater number of molecules of test vapor enter into multi-layered nanotubes with respect to single layer nanotubes. Thus, effective concentration of test vapor in multi-layered nanotubes was relatively larger than single layered nanotubes. Also, capacitive response of the sensor had a logarithmic (non-linear) relationship with the concentration (100-300 ppm) of methanol and ethanol as discussed in Chapter 3. Thus, for the lower ppm level of target vapor (methanol and ethanol in this case), the difference/gap between sensitivities of two vapor was less but this difference/gap keeps on increasing with the concentration. Thus, for single layered nanotubes, the difference between the sensitivity of the sensor towards VOCs was less. But for the same ppm level, since multi-layered nanotubes had a larger concentration of test vapor, therefore, the difference between the sensitivity of the sensor towards VOCs was larger. Since, selectivity essentially measures the difference between the sensitivity of test vapor and interfering vapor; thus, selectivity of the sensor gets enhanced with an increase in the number of layers of nanotubes.

4. 8 Conclusions

This work concerns about developing highly sensitive and selective VOC sensors operating at room temperature (27 °C) with moderate response and recovery time. Developed multi-layered nanotubes sensors have shown high sensitivity towards low concentration (40-160 ppm) of VOCs like ethanol and methanol. The measurement of

resistive response in multi-layer nanotubes sensor has shown two distinctive improvements: (i.) low temperature sensing, and (ii.) high response magnitude. RRM of the sensor gets enhanced with an increase in number of layer(s) and found to be maximum for triple-layered nanotubes. The porous interlayer junction between two layers of nanotubes and Schottky barrier lowering significantly enhanced the resistive sensitivity of multi-layered sensors. However, CRM of the sensor exhibited opposite trends as CRM gets reduced from single layer to double layered nanotubes and further to triple layered nanotubes. An increment in the total area consumed by TiO_2 nanotubes and reduction in vacant space between two electrodes resulted in the reduction of CRM. Also, multi-layered nanotubes exhibited better methanol sensitivity in the capacitive mode with respect to the resistive mode of sensing. Thus, multi layered TiO_2 nanotubes can be considered as a capable gas/vapor sensing material for low or room temperature sensing.

References

1. Y. Gönüllü, A.A. Haidry, and B. Saruhan, Nanotubular Cr-doped TiO_2 for use as high-temperature NO_2 gas sensor, Sensors and Actuators B 217 (2015) 78-87.
2. S. Wang, Z. Lin, W. Wang, C.L. Kuo, K. Hwang, C. Hong, Self-regenerating photocatalytic sensor based on dielectrophoretically assembled TiO_2 nanowires for chemical vapor sensing, Sensors and Actuators B 194 (2014) 1-9.
3. S. Banerjee, S.K. Mohapatra, M. Misra, I.B. Mishra, The detection of improvised non-military peroxide based explosives using a titania nanotube array sensor, Nanotechnology 20 (2009) 075502.
4. Y. Liu, L. Wang, H. Wang, M. Xiong, T. Yang, G.S. Zakharova, Highly sensitive and selective ammonia gas sensors based on PbS quantum dots/TiO_2 nanotube arrays at room temperature, Sensors and Actuators B 236 (2016) 529-536.
5. H. Liu, D. Ding, C. Ning, Z. Li, Wide-range hydrogen sensing with Nb-doped TiO_2 nanotubes, Nanotechnology 23 (2012) 015502.
6. J. Esmaeilzadeha, E. Marzbanrada, C. Zamanib, B. Raissia, Fabrication of undoped-TiO_2

nanostructure-based NO_2 high temperature gas sensor using low frequency AC electrophoretic deposition method, Sensors and Actuators B 161 (2012) 401-405.

7. E. Sennik, N. Kilinc, Z.Z. Ozturk, Electrical and VOC sensing properties of anatase and rutile TiO_2 nanotubes, J. Alloys and Compounds 616 (2014) 89-96.
8. A. Hazra, P. Bhattacharyya, Tailoring of the gas sensing performance of TiO_2 nanotubes by 1-D vertical electron transport technique, IEEE Trans. Electron Devices 61 (2014) 3483-3489.
9. T. Ali, P. Tripathi, A. Azam, W. Raza, A.S. Ahmed, A. Ahmed, M. Muneer, Photocatalytic performance of Fe-doped TiO_2 nanoparticles under visible-light irradiation, Mater. Res. Express 4 (2017) 015022.
10. S. Zhang, M. Yu, L. Xu, S. Zhao, J. Che, X. Zhu, Formation mechanism of multilayer TiO_2 nanotubes in HBF_4 electrolyte, RSC Adv. 7 (2017) 33526-33531.
11. A. Hazra, B. Bhowmik, K. Dutta, V. Manjuladevi, R. K. Gupta, P. P. Chattopadhyay, P. Bhattacharyya, Formation mechanism of anodically grown free-standing TiO_2 nanotube array under the influence of mixed electrolytes, Sci. Adv. Mater. 6 (2014) 714-719.
12. A. Hazra, B. Bhowmik, K. Dutta, V. Manjuladevi, R.K. Gupta, P. Bhattacharyya, Low temperature methanol sensing by p-type nano-titania: correlation with defects states and Schottky barrier model, IEEE Trans. Nanotechnology 14 (2015) 187-195.